Article

Effects of composite oxide supports on catalytic performance of Ni-based catalysts for CO methanation

ZHANG Han [a], DONG Yunyun [b], FANG Weiping [b,*], LIAN Yixin [b,#]

[a] *Department of Chemical and Biochemical Engineering, College of Chemistry and Chemical Engineering, Xiamen University, Xiamen 361005, Fujian, China*
[b] *Department of Chemistry, College of Chemistry and Chemical Engineering, National Engineering Laboratory for Green Chemical Productions of Alcohols-Ethers-Esters, Xiamen University, Xiamen 361005, Fujian, China*

ARTICLE INFO

ABSTRACT

Metal-oxide-modified NiO/Al_2O_3 catalysts for methanation of CO were prepared using a modified grinding-mixing method and characterized using X-ray diffraction, transmission electron microscopy, N_2 adsorption-desorption isotherms, temperature-programmed reduction by H_2, temperature-programmed desorption by H_2, Raman spectroscopy, and X-ray photoelectron spectroscopy. The results show that the activity of an MgO-modified NiO/Al_2O_3 catalyst is better than those of $NiO/ZrO_2-Al_2O_3$ and $NiO/SiO_2-Al_2O_3$ in the reaction temperature range 300–700 °C. The incorporation of a metal oxide into NiO/Al_2O_3 was found to weaken Ni–Al interactions, leading to generation of large numbers of active Ni species, and this was confirmed to be responsible for the improvement in the performances of the catalysts in the methanation reaction.

© 2013, Dalian Institute of Chemical Physics, Chinese Academy of Sciences. Published by Elsevier B.V. All rights reserved.

1. Introduction

In recent years, as oil and natural gas resources have become increasingly scarce [1–3], scientists and engineers in related fields have paid more attention to clean technologies for coal conversion. The conversion of coal to synthetic natural gas has been investigated in parallel with processes for converting coal to liquid fuels and light olefins [4]. The CO methanation reaction, the simplest Fischer-Tropsch synthesis reaction, has the advantages of a high calorific value and environmental friendliness. CO methanation, with methane (CH_4) as the main product, has therefore become an important alternative source of natural gas, and this reaction has been the subject of much research [5–9]. The development of efficient catalysts for CO methanation is therefore important.

There are many metallic elements which are suitable for use as catalysts for CO methanation, e.g., Ru [10], Pt [11], Co [12], and Ni [13]. It is well known that noble-metal catalysts, such as Ru-based catalysts, are excellent for CO methanation, but because of their high cost, large-scale commercialization and industrialization have been restricted [14]. Co-based catalysts tolerate harsh environments well, but have poor selectivity. Ni-based catalysts are superior to Co-based and Fe-based catalysts because of their high catalytic activities, high CH_4 selectivities, and relatively low costs. With these advantages, Ni-based catalysts are promising as good industrial catalysts. However, conventional Ni catalysts supported on alumina are easily deactivated as a result of sintering of Ni particles and coke deposition during the exothermic methanation reaction. Also, to increase their catalytic activities, Ni/Al_2O_3 catalysts usually need to have a high Ni content, which may cause faster deactivation of the catalyst during long-term operation [7,15].

In this work, we focused our attention on the selection of different supports for Ni-based catalysts with low Ni contents for syngas methanation. A series of NiO/MO$_x$-Al$_2$O$_3$ (M = Mg, Si, and Zr) catalysts were prepared using a modified grinding-mixing method. The as-synthesized catalysts were characterized using X-ray diffraction (XRD), transmission electron microscopy (TEM), N$_2$ adsorption-desorption isotherms, temperature-programmed reduction by H$_2$ (H$_2$-TPR), temperature-programmed desorption by H$_2$ (H$_2$-TPD), Raman spectroscopy, and X-ray photoelectron spectroscopy (XPS). The effects of MO$_x$ on the catalytic performances of NiO/MO$_x$-Al$_2$O$_3$ catalysts in the methanation reaction were also investigated.

2. Experimental

2.1. Catalyst preparation

The catalysts were prepared using a modified grinding-mixing method. First, an appropriate amount of nickel nitrate hexahydrate was dissolved in nitric acid solution, followed by blending with an appropriate amount of pseudo-boehmite. After vigorously stirring for 1 h, when an alumina gel formed, a given quantity of alumina powder was added. Then the catalyst precursor was intensively kneaded to produce a paste, extruded to 3 mm × 3 mm cylinders, dried at 120 °C for 12 h, and calcined in air at 500 °C for 4 h. MO$_x$ (M = Mg, Si, Zr) was added simultaneously with pseudo-boehmite to form NiO/MgO-Al$_2$O$_3$, NiO/SiO$_2$-Al$_2$O$_3$, and NiO/ZrO$_2$-Al$_2$O$_3$ catalysts.

2.2. Catalytic activity tests

The methanation reaction was carried out in a continuous-flow quartz fixed-bed reactor at 2.0 MPa in the temperature range 300–700 °C. Typically, the catalyst (0.5 ml, 20–60 mesh) was diluted with ground quartz to prevent it from over-heating as a result of the exothermic reaction. Prior to each experiment, the catalyst was reduced in a flow of H$_2$ for 3 h at 400 °C under a 5% H$_2$ in N$_2$ stream. The reactor was then equilibrated to the desired reaction temperature and the reaction started when the gas flow was switched to syngas (2.0% CO, 25.0% N$_2$, 73.0% H$_2$) with a gas hourly space velocity (GHSV) of 5000 h^{-1}. H$_2$, CO, CH$_4$, and CO$_2$ were monitored using a GC 2060 gas chromatograph. Water in the products was separated by a cold trap before analyzing the product gases. CO conversion and selectivity for CH$_4$ were calculated according to Eqs. (1) and (2), respectively.

$$\text{Conversion of CO} = \frac{\text{moles of reacted CO}}{\text{moles of supplied CO}} \times 100\% \quad (1)$$

$$\text{Selectivity for CH}_4 = \frac{\text{moles of CH}_4 \text{ formed}}{\text{moles of CO reacted}} \times 100\% \quad (2)$$

2.3. Characterization

Powder XRD patterns were recorded using an X'Pert Pro X-ray diffractometer (PANalytical BV, The Netherlands) at a voltage of 40 kV and a current of 30 mA, with Cu K_α radiation. The XRD patterns were referenced to the powder diffraction files (ICDD-FDP data base) for the identification of the peaks.

TEM was performed using a Tecnai F30 high-resolution transmission electron microscope. Samples for TEM observations were suspended in ethanol and dispersed ultrasonically.

The surface textural properties were measured using a Micromeritics TriStar 3000 porosimetry analyzer at –196 °C, using liquid N$_2$. Before physical N$_2$ adsorption of the samples, they were degassed under vacuum at 300 °C for 3 h in a separate degassing unit attached to the instrument. The specific surface area was calculated using the Brunauer-Emmett-Teller (BET) method. The pore size distribution was evaluated using the Barrett-Joyner-Halenda method.

H$_2$-TPR was carried out in a quartz-tube fixed-bed microreactor system. The sample (50 mg) was pretreated at 300 °C for 1 h under an Ar flow (30 ml/min). After cooling to 50 °C, the sample was exposed to a flow (40 ml/min) of 5% H$_2$-95% Ar and ramped to 800 °C at a heating rate of 10 °C/min. The effluent was monitored using a GC 950 gas chromatograph equipped with a thermal conductivity detector.

H$_2$-TPD experiments were performed using Quantachrome equipment. The catalyst (100 mg) was placed in an adsorption vessel and pretreated in Ar (50 ml/min) at 300 °C for 1 h, and then heated to 400 °C and kept at this temperature for 60 min in H$_2$ (30 ml/min). After cooling to 50 °C, H$_2$ was passed over the sample for 30 min. The sample was then swept with Ar for 60 min and finally the desorption step was performed from 50 to 800 °C at a heating rate of 10 °C/min and with an Ar flow of 10 ml/min. The desorbed products were monitored by mass spectrometry.

Raman characterization of the catalysts was carried out on a LabRam I (Jobin-Yvon) at room temperature. Spectra were recorded using the 514.5-nm excitation line of an He-Ne ion laser.

The electronic states of the fresh catalysts were determined by XPS (PHI Quantum 2000 Scanning ESCA Microprobe) using a monochromatic microfocused Al X-ray source. The binding energies were calibrated using C 1s as the reference energy (C 1s = 284.6 eV).

3. Results and discussion

3.1. Catalytic performance

Figure 1 shows the catalytic activities of the catalysts NiO/MO$_x$-Al$_2$O$_3$ in terms of CO conversion and CH$_4$ selectivity. It can be seen from Fig. 1(a) that the CO conversions by the NiO/MO$_x$-Al$_2$O$_3$ catalysts gradually increase with increasing temperature from 300 to 700 °C. The NiO/Al$_2$O$_3$ catalyst shows much lower CO conversion than the other catalysts, indicating that incorporating MgO, SiO$_2$, or ZrO$_2$ into the NiO/Al$_2$O$_3$ catalyst significantly increases its methanation activity, especially at low temperatures. The catalytic performances of the NiO/MO$_x$-Al$_2$O$_3$ catalysts were different, depending on the second metal oxide (MO$_x$) added. The order of the catalytic activities of the NiO/MO$_x$-Al$_2$O$_3$ catalysts is NiO/MgO-Al$_2$O$_3$ > NiO/ZrO$_2$-Al$_2$O$_3$ > NiO/SiO$_2$-Al$_2$O$_3$ > NiO/Al$_2$O$_3$. At 500 °C, the CO conversion by NiO/MgO-Al$_2$O$_3$ reaches 99.6%, which is
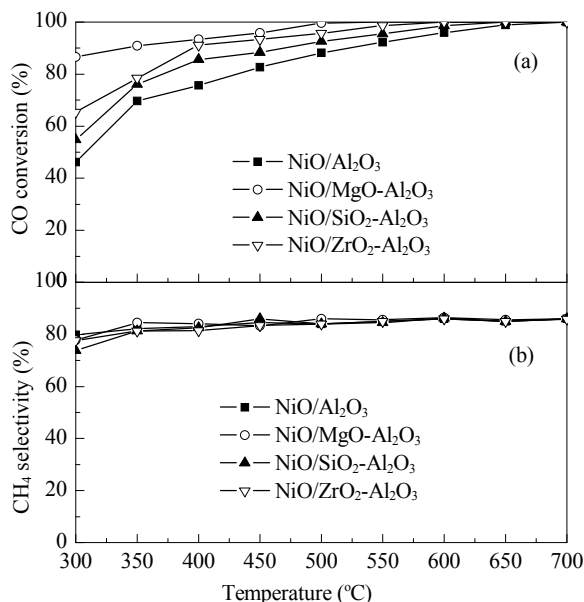
Fig. 1. CO conversion (a) and CH$_4$ selectivity (b) over NiO/MO$_x$-Al$_2$O$_3$ catalysts as a function of reaction temperature. Reaction conditions: 2 MPa, GHSV = 5000 h^{-1}.

higher than those of NiO/ZrO$_2$-Al$_2$O$_3$ (95.7%) and NiO/SiO$_2$-Al$_2$O$_3$ (92.6%). It is observed from Fig. 1(b) that the CH$_4$ selectivities of different NiO/MO$_x$-Al$_2$O$_3$ catalysts are similar to each other in the temperature range 350–700 °C, and are as high as 80%.

3.2. Catalyst characterization

3.2.1. XRD and TEM analysis of Ni-based catalysts

The XRD patterns of Al$_2$O$_3$ and the Ni-based catalysts supported on Al$_2$O$_3$ reduced at 400 °C are displayed in Fig. 2. For Al$_2$O$_3$, the three broad diffraction peaks of γ-Al$_2$O$_3$ are clearly present. No other diffraction peaks arising from the NiO/Al$_2$O$_3$, NiO/MgO-Al$_2$O$_3$, and NiO/SiO$_2$-Al$_2$O$_3$ catalysts are seen, i.e., no clear characteristic diffraction peaks corresponding to free Ni species are detected [16], indicating that NiO is highly dispersed on the surface of the catalysts and small grains that are below the detection limit of XRD measurements are formed [17,18].

To examine the dispersion and morphologies of Ni on the supports, TEM analysis was performed on a series of supported catalysts. The TEM images in Fig. 3 all show that the NiO particles are uniformly dispersed on the supports. This is in agreement with the XRD results. One possible reason is the relatively
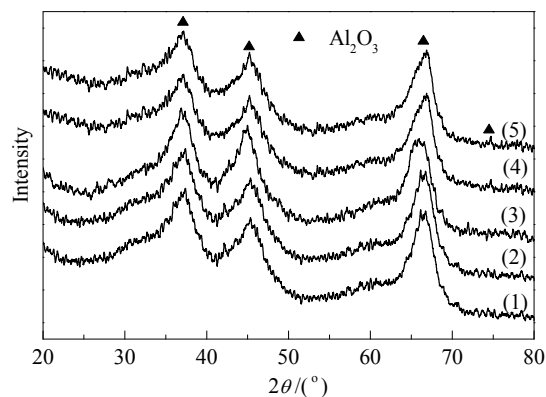

Fig. 2. XRD patterns of reduced Ni-based catalysts and Al$_2$O$_3$. (1) Al$_2$O$_3$; (2) NiO/Al$_2$O$_3$; (3) NiO/MgO-Al$_2$O$_3$; (4) NiO/SiO$_2$-Al$_2$O$_3$; (5) NiO/ZrO$_2$-Al$_2$O$_3$.

low Ni loadings. The differences among these catalysts could not be seen from the XRD and TEM analyses, so other characterization methods were used.

3.2.2. N$_2$ adsorption-desorption isotherms

The N$_2$ adsorption-desorption isotherms of different NiO/MO$_x$-Al$_2$O$_3$ catalysts are shown in Fig. 4. Clearly, all the isotherms are type IV, which is characteristic of a mesoporous structure with a hysteresis loop. This type of loop is usually ascribed to ink-bottle pores, with narrow orifices and broader inner parts [19]. The BET surface areas, average pore sizes, and pore volumes of the NiO/MO$_x$-Al$_2$O$_3$ catalysts are summarized in Table 1. The specific surface area of NiO/Al$_2$O$_3$ is 192 m^2/g. It decreased to 159 m^2/g after the addition of MgO. Generally, the higher the surface area is, the higher the catalytic performance is, but this is not consistent with our observations. The work of Guo et al. [20] and the evaluation results for our catalysts show that the catalyst area is not directly related to the catalytic activity for CO methanation in this system. It is the chemical properties, rather than the physical properties, that mainly determine the catalyst performance.

3.2.3. H$_2$-TPD characterization

Figure 5 shows the H$_2$-TPD profiles of the reduced NiO/MO$_x$-Al$_2$O$_3$ catalysts. All the profiles show a very small hydrogen desorption peak in the temperature range 150–350 °C and a broad hydrogen desorption peak in the temperature range 400–700 °C, which can be ascribed to dominant hydrogen adsorption at active sites on the Ni grain surfaces. The intensities of the Ni–Al interactions in these four catalysts are
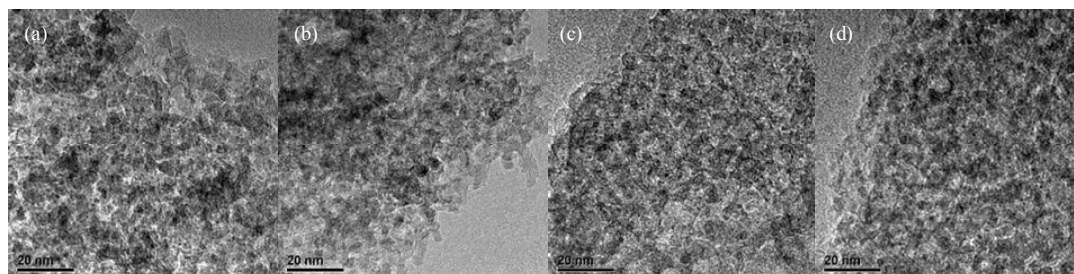

Fig. 3. TEM images of different NiO/MO$_x$-Al$_2$O$_3$ catalysts. (a) NiO/Al$_2$O$_3$; (b) NiO/MgO-Al$_2$O$_3$; (c) NiO/SiO$_2$-Al$_2$O$_3$; (d) NiO/ZrO$_2$-Al$_2$O$_3$.
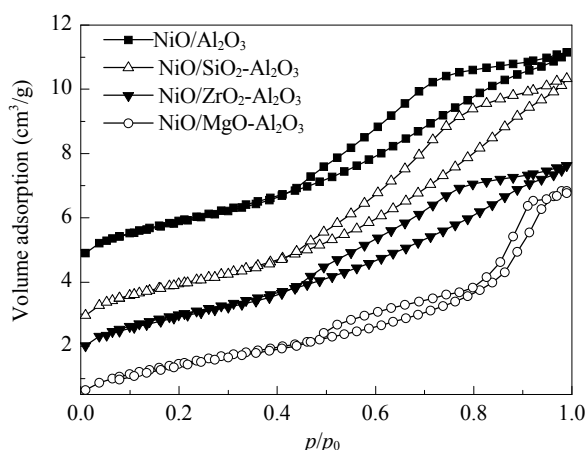
Fig. 4. N_2 adsorption-desorption isotherms of NiO/MO_x-Al_2O_3 catalysts calcined at 500 °C.

Table 1
Surface areas, pore volumes, and average pore diameters of fresh NiO/MO_x-Al_2O_3 catalysts.

Catalyst	BET surface area (m²/g)	Pore volume (cm³/g)	Pore diameter (nm)
NiO/Al_2O_3	192	0.26	4.6
NiO/MgO-Al_2O_3	159	0.25	6.0
NiO/SiO_2-Al_2O_3	193	0.30	5.4
NiO/ZrO_2-Al_2O_3	186	0.24	4.6

different, but they are generally high, and the Ni loadings are low. All these factors lead to the small hydrogen desorption peak in the low-temperature range. Among the catalysts tested, NiO/MgO-Al_2O_3 exhibits the highest peak intensity. This can be attributed to larger amounts of active Ni species. The amount of desorbed hydrogen, corresponding to the peak area, depends on the second metal oxide added and increases in the order NiO/Al_2O_3 < NiO/SiO_2-Al_2O_3 < NiO/ZrO_2-Al_2O_3 < NiO/MgO-Al_2O_3. The area of the H_2-TPD peak correlates well with the amount of active Ni species. The larger the peak area and the larger the amount of hydrogen adsorbed, the higher the catalytic activity [21]. From the mechanism of CO methanation [22,23], we know that the amount of hydrogen involved in the methanation reaction is one of the crucial factors determining
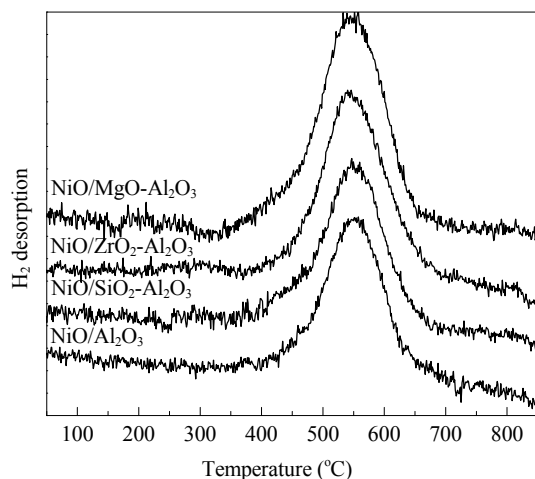
catalytic performance. In a hydrogen atmosphere, surface carbon and oxygen species formed through CO dissociation are speedily converted to CH_4 and CO_2 and desquamate from the surface to provide adsorption centers for further CO adsorption, thereby accelerating CO adsorption [24,25]. An increase in hydrogen adsorption could therefore enhance CO adsorption on the catalyst surface, promoting activation of hydrogen and CO [26]. As a result, the catalyst performance will be improved.

3.2.4. H_2-TPR characterization

H$_2$-TPR characterization was conducted to understand the reducibilities and the optimum reduction temperatures for the Ni-based catalysts. All the H_2-TPR experiments ended at a temperature of 800 °C, as shown in Fig. 6. Two reduction peaks were observed in the H_2-TPR profiles. The reduction peaks that appeared in the temperature range 300–450 °C, with an optimum temperature at around 400 °C, can be ascribed partly to NiO and partly to Ni^{2+} species weakly interacting with the support. The reduction peaks observed in the temperature range 500–800 °C, with an optimum temperature at around 700 °C, probably correspond to the reduction of Ni^{2+} in the $NiAl_2O_4$ phase [6,27–29] or to Ni interacting strongly with the support. This $NiAl_2O_4$ spinel phase has a stable structure and is difficult to reduce to Ni^0 species at low temperatures. In general, the changes in the optimum reduction temperature reflect the extent of interactions between the active component and the support. The temperature at which the first reduction peak appeared shifted downwards from 402 to 378 °C, suggesting that the reduction of NiO to Ni^0 becomes easier after Mg, Si, or Zr addition, and the active Ni component in the NiO/Al_2O_3 catalyst has stronger interactions with the support and is more difficult to reduce compared with the other NiO/MO_x-Al_2O_3 catalysts.

The catalyst reduction ability is directly related to the amount of free nickel-oxide species. For NiO/Al_2O_3, there may be only a few free nickel-oxide species in the catalyst. However, NiO/MgO-Al_2O_3 has many free nickel-oxide species, and these make reduction of the catalyst easier at low temperatures. As can be seen from Fig. 5, the intensities of the peaks arising from NiO in NiO/MO_x-Al_2O_3 are in the order NiO/MgO–Al_2O_3 >
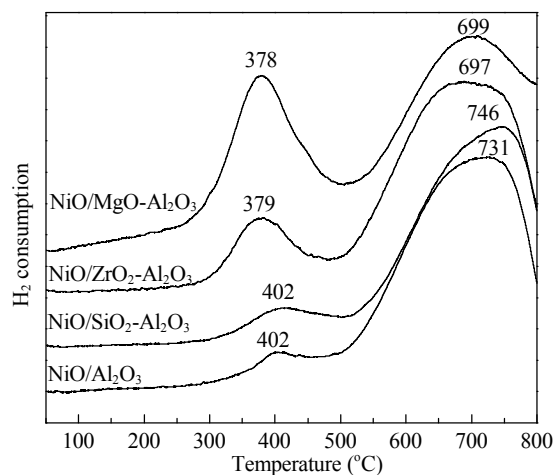

Fig. 5. H_2-TPD profiles of the reduced NiO/MO_x-Al_2O_3 catalysts.

Fig. 6. H_2-TPR profiles of the NiO/MO_x-Al_2O_3 catalysts.
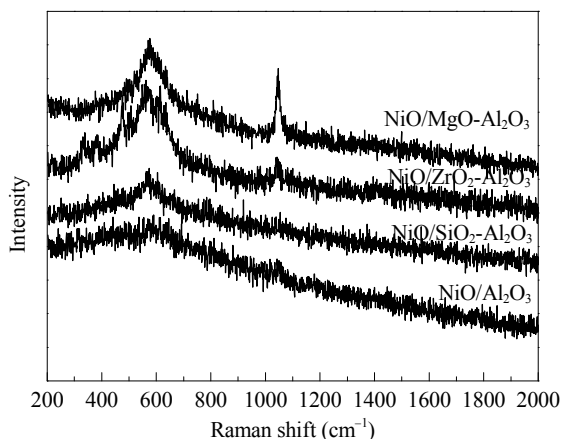
Fig. 7. Raman spectra of the NiO/MO$_x$-Al$_2$O$_3$ catalysts.

NiO/ZrO$_2$-Al$_2$O$_3$ > NiO/SiO$_2$-Al$_2$O$_3$ > NiO/Al$_2$O$_3$. This is in good agreement with those obtained from Raman characterization (Fig. 7).

3.2.5. Raman spectra

Figure 7 shows the Raman spectra for the NiO/MO$_x$-Al$_2$O$_3$ catalysts. It is well known that the only phase of alumina that exhibits Raman bands is α-Al$_2$O$_3$ [22]. In our present work, the catalysts were calcined at 500 °C, and only the γ-Al$_2$O$_3$ phase was formed, from which no Raman bands would be observed [22,23]. For the NiO/MO$_x$-Al$_2$O$_3$ catalysts, there are two explicit Raman peaks, at around 546 and 1092 cm^{-1}, as shown in Fig. 7. Based on previous results [21,30], these two peaks are the characteristic bands of the first-order longitudinal optical (LO) phonon modes of cubic NiO single-crystals and a combination of 2LO modes, respectively. The amounts of active free Ni species on the surfaces of the catalysts could therefore be estimated by comparing the intensities of these two NiO Raman peaks [31]. The peak intensity specific to free nickel-oxide species in NiO/MgO-Al$_2$O$_3$ is the strongest. Only a weak NiO signal peak was observed for NiO/Al$_2$O$_3$, suggesting that there is little NiO on the surface of this catalyst. One reason is that large amounts of NiO species could enter into the support during preparation and pretreatment [32]. It is therefore reasonable to conclude

that addition of a metal oxide to NiO/Al$_2$O$_3$ will favor formation of active free Ni species.

3.2.6. XPS analysis

XPS spectra specific to Ni 2$p_{3/2}$ and Al 2p of the catalysts are presented in Fig. 8. Figure 8(a) shows the existence of two types of Ni species, corresponding to the main peaks at around 854 and 860 eV. From the H$_2$-TPR results, it can be inferred that there might be NiO and NiAl$_2$O$_4$ on the catalyst surfaces [27]. The former is characterized by weak interactions with the support [33]. The latter may be NiAl$_2$O$_4$ or Ni^{2+}, which are characterized by strong interactions with the support. It has been noted that the binding energy of the Ni 2$p_{3/2}$ peak arising from NiO/Al$_2$O$_3$ was higher than that for the others, as a result of stronger interactions between Ni and the support. However, the binding energy of Ni in the NiO/MgO-Al$_2$O$_3$ catalyst shifted down by the largest extent, followed by NiO/ZrO$_2$-Al$_2$O$_3$ and NiO/SiO$_2$-Al$_2$O$_3$. This implies that when another metal oxide is added to the NiO/Al$_2$O$_3$ catalyst, the interactions between the active component, i.e., NiO, and the support will be weakened. This speculation is in line with the XPS spectra specific to Al 2p (Fig. 8(b)). As can be seen from the curves, the binding energy of the Al 2p peak for NiO/Al$_2$O$_3$ is at 74 eV, which is typical of Al^{3+} in the spinel phase [34], but for NiO/MgO-Al$_2$O$_3$, the binding energy is smaller.

4. Conclusions

NiO/Al$_2$O$_3$ catalysts for CO methanation can be promoted by the addition of metal oxides, namely MgO, SiO$_2$, and ZrO$_2$. MgO was found to be the most efficient promoter, giving a CO conversion as high as 99.6% at 500 °C. In the NiO/MgO-Al$_2$O$_3$ catalyst, the Ni–Al interactions are significantly weakened and consequently reduction of the catalyst at low temperatures is easy, leading to generation of more free nickel-oxide species on the catalyst surface.

References

[1] Kopyscinski J, Schildhauer T J, Biollaz S M. *Fuel*, 2010, 89: 1763
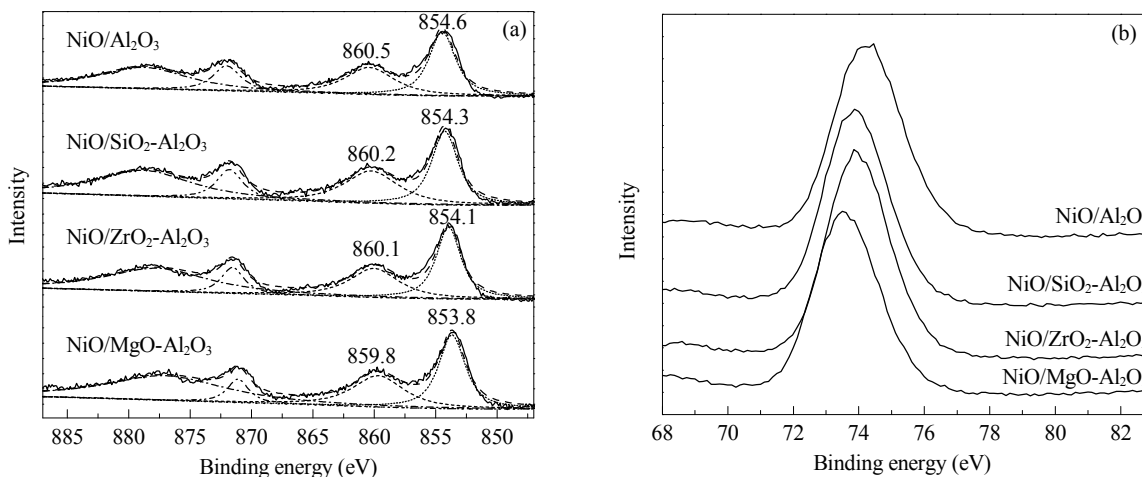

**Fig. 8.** Ni 2$p_{3/2}$ (a) and Al 2p (b) XPS spectra of NiO/MO$_x$-Al$_2$O$_3$.

Graphical Abstract

Effects of composite oxide supports on catalytic performance of Ni-based catalysts for CO methanation

ZHANG Han, DONG Yunyun, FANG Weiping*, LIAN Yixin*
Xiamen University

NiO/MO$_x$-Al$_2$O$_3$ (M = Mg, Si, Zr) catalysts for CO methanation, prepared using a modified grinding-mixing method, have higher catalytic activities than that of a conventional NiO/Al$_2$O$_3$ catalyst. This is attributed to the weakening of Ni–Al interactions after adding MO$_x$.
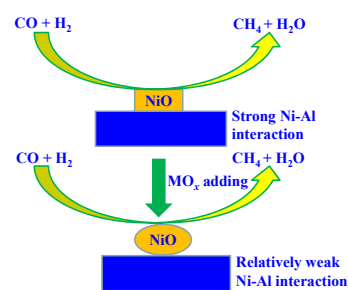
[2] Wu R F, Wang Y Z, Gao C G, Zhao Y X. *J Fuel Chem Technol*, 2009, 37: 578

[3] Turner J A. *Science*, 2004, 305: 972

[4] Huffman G P. *Fuel*, 2011, 90: 2671

[5] Zhao A, Ying W, Zhang H, Ma H, Fang D. *Catal Commun*, 2012, 17: 34

[6] Liu Z, Chu B, Zhai X, Jin Y, Cheng Y. *Fuel*, 2012, 95: 599

[7] Wang S H, Lee J, Hong U G, Jung J C, Koh D J, Lim H, Byun C, Song I K. *J Ind Eng Chem*, 2002, 18: 243

[8] Takenaka S, Shimizu T, Otsuka K. *Int J Hydrogen Energy*, 2004, 29: 1065

[9] Urasaki K, Endo K I, Takahiro T, Kikuchi R, Kojima T, Satokawa S. *Top Catal*, 2010, 53: 707

[10] Galletti C, Specchia S, Specchia V. *Chem Eng J*, 2011, 167: 616

[11] Bajusz J G, Kwik D J, Goodwin J G. *Catal Lett*, 1997, 48: 151

[12] Kok E, Scott J, Cant N, Trimm D. *Catal Today*, 2011, 164: 297

[13] Kim S H, Nam S W, Lim T H, Lee H I. *Appl Catal B*, 2008, 81: 97

[14] Duan X, Qian G, Zhou X, Sui Z, Chen D, Yuan W. *Appl Catal B*, 2011, 101: 189

[15] Kelley R D, Candela G A, Madey T E, Newbury D E, Schehl R R. *J Catal*, 1983, 80: 235

[16] Song H L, Yang J, Zhao J, Chou L J. *Chin J Catal* (宋焕玲, 杨建, 赵军, 丑凌军. 催化学报), 2010, 31: 21

[17] Zhao A M, Ying W Z, Zhang H T, Ma H F, Fang D Y. *J Nat Gas Chem*, 2012, 21: 170

[18] Ma S L, Tan Y S, Han Y Z. *J Nat Gas Chem*, 2011, 20: 435

[19] Wang J, Wang Y, Wen J, Shen M, Wang W. *Microporous Mesoporous Mater*, 2009, 121: 208

[20] Guo J, Lou H, Zhao H, Chai D, Zheng X. *Appl Catal A*, 2004, 273: 75

[21] Dietz R E, Parisot G I, Meixner A E. *Phys Rev B*, 1971, 4: 2302

[22] Aminzadeh A, Sarikhani-Fard H. *Spectrochim Acta Part A*, 1999, 55A: 1421

[23] Mortensen A, Christensen D H, Nielsen O F, Pedersen E. *J Raman Spectrosc*, 1991, 22: 47

[24] Alstrup I. *J Catal*, 1995, 151: 216

[25] Yadav R, Rinker R G. *Ind Eng Chem Res*, 1992, 31: 502

[26] Dai X P, Yu C C. *J Nat Gas Chem*, 2008, 17: 365

[27] Cai M D, Wen J, Chu W, Cheng X Q, Li Z J. *J Nat Gas Chem*, 2011, 20: 318

[28] Seo J G, Youn M H, Song I K. *J Mol Catal A*, 2007, 268: 9

[29] Yang J, Wang X, Li L, Shen K, Lu X, Ding W. *Appl Catal B*, 2010, 96: 232

[30] Wang W Z, Liu Y K, Xu C K, Zheng C L, Wang G H. *Chem Phys Lett*, 2002, 362: 119

[31] Liu S L, Xiong G X, Yang W S, Xu L Y, Xiong G, Li C. *Catal Lett*, 1999, 63: 167

[32] Maluf S S, Assaf E M. *Fuel*, 2009, 88: 1547

[33] Guimon C, Auroux A, Romero E, Monzon A. *Appl Catal A*, 2003, 251: 199

[34] Ashok J, Raju G, Reddy P S, Subrahmanyam M, Venugopal A. *Int J Hydrogen Energy*, 2008, 33: 4809

复合氧化物载体对镍基催化剂上CO甲烷化反应性能的影响

张　罕[a], 董云芸[b], 方维平[b,*], 连奕新[b,#]
[a]厦门大学化学化工学院化学工程与生物工程系, 福建厦门 361005
[b]厦门大学化学化工学院化学系, 醇醚酯化工清洁生产国家工程实验室, 福建厦门 361005

摘要: 采用改良的粉末混合法制备了系列经过其它金属氧化物改性的NiO/Al$_2$O$_3$催化剂, 并运用X射线衍射、透射电子显微镜、N$_2$低温物理吸附-脱附、程序升温还原、程序升温脱附、拉曼以及X射线光电子能谱对催化剂进行了表征. 结果显示, 在300~700 °C经MgO修饰的NiO/Al$_2$O$_3$催化剂上CO甲烷化反应活性比NiO/ZrO$_2$-Al$_2$O$_3$和NiO/SiO$_2$-Al$_2$O$_3$的高. 另一金属氧化物的加入削弱了NiO/Al$_2$O$_3$催化剂中Ni-Al间相互作用, 形成更多的活性Ni物种, 从而促进了反应的进行.
关键词: 一氧化碳; 甲烷化; 镍基催化剂; 合成气; 复合氧化物载体